Cancer Research

The miR-146b-3p/PAX8/NIS Regulatory Circuit Modulates the Differentiation Phenotype and Function of Thyroid Cells during Carcinogenesis

Garcilaso Riesco-Eizaguirre[1,2,3], León Wert-Lamas[1], Javier Perales-Patón[1,4], Ana Sastre-Perona[1], Lara P. Fernández[1], and Pilar Santisteban[1]

Abstract

The presence of differentiated thyroid cells in thyroid cancer is critical for the antitumor response to radioactive iodide treatment, and loss of the differentiated phenotype is a key hallmark of iodide-refractory metastatic disease. The role of microRNAs (miRNA) in fine-tuning gene expression has become a major regulatory mechanism by which developmental and pathologic processes occur. In this study, we performed next-generation sequencing and expression analysis of eight papillary thyroid carcinomas (PTC) to comprehensively characterize miRNAs involved in loss of differentiation. We found that only a small set of abundant miRNAs is differentially expressed between PTC tissue and normal tissue from the same patient. In addition, we integrated computational prediction of potential targets and mRNA sequencing and identified a master miRNA regulatory network involved in essential biologic processes such as thyroid differentiation. Both mature products of mir-146b (miR-146b-5p and -3p) were among the most abundantly expressed miRNAs in tumors. Specifically, we found that miR-146b-3p binds to the 3′-untranslated region of PAX8 and sodium/iodide symporter (NIS), leading to impaired protein translation and a subsequent reduction in iodide uptake. Furthermore, our findings show that miR-146b and PAX8 regulate each other and share common target genes, thus highlighting a novel regulatory circuit that governs the differentiated phenotype of PTC. In conclusion, our study has uncovered the existence of a miR-146b-3p/PAX8/NIS regulatory circuit that may be exploited therapeutically to modulate thyroid cell differentiation and iodide uptake for improved treatment of advanced thyroid cancer. *Cancer Res; 75(19); 4119–30. ©2015 AACR.*

Introduction

Thyroid cancer has in general terms a good prognosis, as the majority of the patients with this disease can be cured with surgery and radioactive iodide treatment. The ability of differentiated thyroid cells to accumulate iodide is clinically highly relevant because it makes it possible for patients with thyroid cancer to be treated with ablative doses of radioactive iodide after an adequate stimulation by thyroid-stimulating hormone (TSH; ref. 1). However, some patients develop metastatic disease refractory to radioactive iodide treatment and their life expectancy significantly decreases. Thus, the maintenance of the thyroid differentiated phenotype during tumor transformation has a critical impact in thyroid cancer patient's survival (2).

The maintenance of the thyroid differentiated phenotype requires the presence of PAX8, a member of the paired box (PAX) family of transcription factors (TF; ref. 3). Together with the other thyroid TFs NKX2-1 and FOXE1, PAX8 is involved in thyroid follicular cell development and expression of thyroid-specific genes such as the sodium/iodide symporter (*SLC5A5*, also named as *NIS*), thyroglobulin (*Tg*), and thyroperoxidase (*TPO*; refs. 4, 5). These genes are essential for thyroid differentiation as they mediate the metabolism of iodide, leading to the synthesis of active thyroid hormone. One of the most important and well-established transcriptional targets of PAX8 is NIS. This symporter is a key plasma membrane protein that mediates active iodide transport in the thyroid and other tissues (6). In the healthy thyroid, NIS-mediated iodide uptake is the first step in thyroid hormone biosynthesis. NIS also plays a central role in thyroid cancer treatment. As long as a few NIS molecules are functionally expressed in thyroid cancer cells, thyroid cancer is successfully treated by thyroidectomy followed by radioactive iodide (^{131}I) administration. Radioactive iodide selectively targets and destroys any remnant or metastatic NIS-expressing thyroid cancer cells. Radioactive iodide treatment is the most effectively targeted internal radiation anticancer therapy ever devised and it has been in use for over 60 years. Therefore, loss of the thyroid differentiated phenotype, particularly loss of NIS function, is one of the most important hallmarks of thyroid cancer progression, leading to iodide-refractory metastatic disease and a worse outcome of the patients (7, 8).

[1]Instituto de Investigaciones Biomédicas "Alberto Sols," Consejo Superior de Investigaciones Científicas and Universidad Autónoma de Madrid (CSIC-UAM), Madrid, Spain. [2]Servicio de Endocrinología y Nutrición, Hospital Universitario La Paz, IdiPAZ, Madrid, Spain. [3]Servicio de Endocrinología Hospital Universitario de Móstoles, Madrid, Spain. [4]Translational Bioinformatics Unit, Clinical Research Programme, Spanish National Cancer Research Centre (CNIO), Madrid, Spain.

Note: Supplementary data for this article are available at Cancer Research Online (http://cancerres.aacrjournals.org/).

G. Riesco-Eizaguirre and L. Wert-Lamas contributed equally to this article.

Corresponding Author: Pilar Santisteban, Instituto de Investigaciones Biomédicas, Consejo Superior de Investigaciones Científicas and Universidad Autónoma de Madrid (CSIC-UAM), C/Arturo Duperier 4, 28029 Madrid, Spain. Phone: 34-91-585-4455; Fax: 34-91-585-4401; E-mail: psantisteban@iib.uam.es

doi: 10.1158/0008-5472.CAN-14-3547

MicroRNAs (miRNA) inhibit translation or induce mRNA degradation in general by binding to the 3′-untranslated region (3′-UTR) of target mRNAs. Since initial observation, about 3,000 human miRNAs have been registered in miRBase (v.20.0; ref. 9) and are thought to regulate 50% of the transcriptome. Although a previous classical approach of cloning has partially revealed miRNA expression profile in thyroid tumors (10, 11), low throughput with low sensitivity and poor resolution makes these approaches limited to define miRNome. Genome-wide sequencing of miRNAs can identify miRNome in-depth, which reveals miRNA expression differences as well as the individual miRNA abundance. As a minimum threshold amount must be reached for miRNAs to repress target mRNAs (12–15), the abundance of miRNAs and their ratios in the entire miRNome of specific cell or tissue may be very important for their functions.

When preparing this article, results from The Cancer Genome Atlas (TCGA) project based on a comprehensive multiplatform analysis of 496 papillary thyroid carcinomas (PTC), the most common type of thyroid cancer, were published (16). In such work, several miRNAs were associated with less differentiated tumors. Here, we took an integrated approach and based on the abundance of the miRNAs and their ratios in the entire miRNome, we analyzed miRNAs and the transcriptome from paired normal and tumor thyroid tissue from 8 patients with PTC. Our aim was to uncover the underlying miRNA regulatory network that determines differentiation in PTCs and to provide functional studies to characterize those miRNAs involved in the modulation of genes essential for thyroid differentiation and iodide uptake, namely *PAX8* and *NIS*.

Materials and Methods

Thyroid tissue samples

For the sequencing experiment, fresh-frozen samples from PTC tumors ($n = 8$) and contralateral normal thyroid tissue from the same patient ($n = 8$) were collected at the Biobank of the Hospital Universitario La Paz (Madrid, Spain). The clinical characteristics of patients are summarized in Supplementary Table S1 and other details in Supplementary Materials and Methods. An independent cohort of 16 samples from PTC tumors was used for validation.

Next-generation sequencing

The sequencing procedure was carried out using the Genome Analyzer IIx Platform (Illumina) at the Genomics Core Unit of CNIO (the Spanish National Cancer Research Centre, Madrid, Spain) using the standard protocols recommended for small RNA-seq (Illumina TruSeq Small RNA) and mRNA-seq (Illumina TruSeq Stranded mRNA). Using Cutadapt software (v. 1.2.1), 3′ adapters from small RNA reads were removed, filtering reads with lengths of 17 to 34 nt. The remaining short reads were aligned to the human genome (UCSC, hg19 assembly) using Bowtie algorithm (v0.12.7; ref. 17) with the criteria of perfect match. Reads mapping on each mature miRNA genomic location were counted using HTSeq-count (v. 0.5.4), toward the miRNA annotation from miRBase version 20 (hg19 assembly, June 2013). Clean sequenced reads (excluding reads containing ambiguous base and adaptor contaminants) were used for further analysis and reads classified as small RNAs from other species [rRNA, tRNA, scRNA, snRNA, snoRNA, repeat-associated small RNAs and mRNAs (exons/introns)] were excluded (Supplementary Fig. S1). The mRNA reads were aligned to the human genome (UCSC, hg19 assembly) using TopHat v.2.0.4 (18), permitting two mismatches and a maximum of five multi-hits. The gene-level expression was calculated as the sum of all read counts over their exons by using Htseq-count and the gene annotation from the reference genome (hg19, UCSC; ref. 19). All sequencing data can be downloaded from Gene Expression Omnibus (GEO) under accession number GSE63511.

Bioinformatic predictions of target genes

TargetScan algorithm (20) was used to predict hypothetical associations between miRNA and mRNA pairs. A second algorithm based on DIANAmicroT was used to validate the predictions (http://www.microrna.gr/microT-CDS). Inverse correlations between expression levels of miRNAs and their putative target genes were calculated using the Pearson correlation test, adjusting for multiple testing (Benjamini and Hochberg method). All significant predictions were integrated in addition of experimentally validated interactions collected from TarBase (v.6), miRecords (v.3), and miRTarbase (v.3) databases. Networks comprising genes and miRNAs were drawn by Cytoscape (21).

RNA quantification

Total RNA was isolated from cells with TRIzol (Invitrogen) according to the manufacturer's instructions. RT-PCR and qRT-PCR were performed as described in Supplementary Materials and Methods.

Cell lines and transfections

PCCl3 cells were grown in Coon's modified Hams F12 medium supplemented with a six-hormone mixture (1 nmol/L TSH, 10 μg/mL insulin, 10 ng/mL somatostatin, 5 μg/mL transferrin, 10 nmol/L hydrocortisone, and 20 ng/mL glycyl-L-histidyl-L-lysine acetate) all from Sigma-Aldrich, and 5% donor calf serum (Life Technologies). Near-confluent cells were starved for TSH and insulin in the presence of 0.2% serum (starvation medium) for 4 days. Then, TSH (0.5 mU/mL) alone or together with IGF1 (100 ng/mL) or TGFβ (10 ng/mL; the last two from PeproTech) were added to the culture medium at 24 hours and RNA was then extracted.

Pax8 silencing was performed either transfecting the cells with Pax8 siRNA or Scrambled conditions (10 ng siRNA/mL; Dharmacon) as described previously (22) or transducing the cells with lentivirus containing short hairpin RNA against Pax8, using a shScramble as control (pGIPZ_Pax8 (clon#V3LHS_408573) and pGIPZ-Scramble, respectively (Open Biosystems). VSV-G pseudotyped lentivirus production was performed as previously described (23). MDCKhNIS cells have been described elsewhere (24) and the human thyroid follicular cell line Nthy-ori 3-1 was obtained from the European Collection of Cell Cultures (ECACC). HeLa cell were grown as described previously (23). Cells stably expressing miRNA are described in Supplementary Materials and Methods. Cell lines were routinely authenticated every 6 months by short tandem repeat (STR) profiles using the Applied Biosystems Identifier kit in the Genomic Facility at the Institute of Biomedical Research (IIBm; Madrid, Spain).

Generation of stably transfected cells

A total of 2.5×10^5, MDCKh NIS or Nthy-ori3-1, cells seeded in 12-well plates were transfected with 1 μg/well miRNA precursor expression vector or the null control vector using calcium

phosphate or the lipid-based transfection agent Fugene6 according to the manufacturer's instructions (Promega). Transfected cells were selected with puromicin and the expression of miRNA detected by GFP and /or qRT-PCR.

Plasmids and constructs

miR-146b and unrelated miRNAs (miR-373, miR-15a) precursors (pre-mir) were cloned into pEGP-miR expression vector (Cell Biolabs), specifically into *Bam*HI and *Nhe*I binding sites. The generated constructs were transfected to MDCKhNIS and Nthy-ori 3-1 cells as described in Supplementary Materials and Methods.

Protein extraction, Western blotting, and antibodies

Cells were lysed in lysis buffer containing 1% Nonidet P-40, 1 mmol/L EDTA, 50 mmol/L Tris–HCl (pH 7.5), and 150 mmol/L NaCl, supplemented with complete protease inhibitors mixture (Roche Diagnostics). All samples were diluted in loading buffer and heated at 90°C for 5 minutes except for NIS, which was heated at 37°C for 30 minutes. Samples were then separated by SDS-PAGE, transferred onto nitrocellulose membrane (Schleicher & Schuell), and immunoreactive proteins visualized by enhanced chemiluminescence (GE Healthcare). Antibodies against hNIS and rNIS were kindly provided by Dr. Carrasco (Yale School of Medicine, New Haven, CT). The antibodies for actin and PAX8 were from Santa Cruz Biotechnology Inc. and BioPat, respectively.

Iodide transport

PCCl3 and MDCKhNIS cells were assayed for iodide transport as previously described (25) and detailed in Supplementary Materials and Methods.

Statistical analysis

A differential expression analysis based on the read counts from the sequencing data was performed using the edgeR package (v.3.2.4; ref. 26). A Trimmed means of *M* values normalization method of the gene-level expression was applied (27). To dampen the multiple testing issues, low-expressed tags were filtered out based on a minimum cutoff level [miR-level of 0.6 "counts per million" (CPM) for small RNA-seq dataset, gene-level of 1 CPM for mRNA-seq dataset] in at least 50% of samples within any biologic group. The negative binomial Generalized Linear Model for a design of paired samples was used to detect genes differentially expressed between PTC and normal tissue. After correcting *P* values for Benjamini and Hochberg method, genes and miRNAs with false discovery rates (FDR) <0.05 were considered as differentially expressed.

The GOseq package (v. 1.12.0; ref. 28) was used to identify overrepresented gene sets defined in KEGG (Kyoto Encyclopedia of Genes and Genomes) among differentially expressed genes. The Wallnius noncentral hypergeometric distribution method was used to approximate the true distribution of members of each gene set among the list of deregulated genes. Gene sets with FDR <0.05 were considered as overrepresented. The results in qRT-PCR, luciferase activity, and iodide uptake are expressed as the mean ± SEM of at least three different experiments performed in triplicate. Statistical significance was determined by the *t* test analysis (two-tailed), and differences were considered significant at a *P* value of <0.05.

Results

Identification of miRNomes in normal thyroid and PTC unveils the most abundant deregulated miRNAs in PTC

To carry out an in-depth analysis of the functional miRNome, we performed next-generation sequencing of small RNA in paired normal and tumor thyroid tissue from 8 patients with PTC, the most common type of thyroid cancer. The abundance value of each known miRNA was normalized using CPM in each small RNA library. Significance analysis of differential miRNA expression and hierarchical clustering analysis clearly separated tumors from normal tissue samples (Supplementary Fig. S1). The miRNAs with >1,000 CPMs were considered to be abundantly expressed and, thus, most likely to be functional (15). We found that approximately 15% of the detected miRNAs were abundantly expressed (81 of 577 in normal thyroid tissues and 77 of 574 in tumor tissues) accounting for 96% of all miRNAs reads (Supplementary Fig. S1 and Supplementary Dataset S1 and S2). The great majority of the most abundant miRNAs (87%) were present in both normal and tumor tissue with no significant variations identifying a thyroid-specific miRNome (Supplementary Fig. S1). Altogether, our sequence analysis accurately classifies normal and tumor tissue and shows that PTC and normal thyroid express a large, highly similar set of abundantly expressed miRNAs that corresponds to the functional miRNome of the thyroid.

We next wanted to know which miRNAs are the major players in PTC pathogenesis. As only a few miRNAs are abundantly expressed in the miRNome and they seem to be the most important in thyroid biology, only miRNAs with CPM >1,000 and more than 1.5-fold change were considered most likely to be important in PTC pathogenesis in this study. We identified a set of 12 upregulated and eight downregulated miRNAs after pair-wise comparison between the eight malignant tumors and their corresponding normal samples (Table 1). In the list of upregulated miRNAs, the most abundant and upregulated by far was miR-146b-5p. Interestingly, miR-146b-3p, formerly thought to be a passenger strand, was also among the most abundant upregulated miRNAs. Because miR-155 and miR-34a are close to the threshold of 1,000 CPMs and have been previously shown to be deregulated in PTC, we decided to consider them as more likely to be functional. On the other hand, as miR-21-3p and miR-181a-2-3p are not included in TargetScan database, they were not considered in this work. In the list of downregulated miRNAs, the three most abundant were miR-451a, miR-486, and miR-100b. Low abundant miRNAs being significantly deregulated in PTC are shown in Supplementary Dataset S2 and, although its biologic relevance remains to be proved, we cannot rule out that they play a functional role. Subsequent validation through qRT-PCR of several deregulated miRNAs was performed in an independent cohort of 16 patients with PTC. (Supplementary Fig. S2A). We also performed next-generation sequencing in eight extra tumors with PTC obtaining similar results (Supplementary Fig. S2B). Together, the miRNomes of human normal thyroid and PTC led us to identify the consistently deregulated miRNA in thyroid cancer.

Identification of a miRNA regulatory network in PTC reveals miRNAs that regulate genes essential for thyroid differentiation

To identify target genes of the most abundant deregulated miRNAs, we first performed next-generation sequencing of mRNA in the paired normal and tumor thyroid tissue from the same 8

patients with PTC. Overall, 910 genes were significantly deregulated (536 were overexpressed and 374 were downregulated; Supplementary Dataset S3). We further characterized the biologic signatures associated with our sequencing analysis. Overrepresentation analysis (ORA) based on the KEGG pathways database revealed enrichment of cell membrane–mediated pathways (Supplementary Table S2), including ECM–receptor interaction, cell adhesion molecules (CAM) and focal adhesion. This finding highlights the role of integrins among other membrane-bound mediators in thyroid malignancy, similar to what has been previously described (29). ORA also revealed enrichment of small cell lung cancer and TGFβ signaling pathways, highlighting the role of these canonical pathways in thyroid cancer.

A single miRNA has been shown to target multiple mRNAs to regulate gene expression. Conversely, the expression of a single gene can be regulated by several miRNAs. Thus, the generation of miRNAs-gene regulatory networks is believed to affect essential cellular functions. To identify target genes of the upregulated miRNAs in PTC, we used the computational target prediction program TargetScan and searched into the 374 downregulated genes in our sequencing analysis. This revealed a shorter list of 217 potential target genes for the upregulated miRNAs in PTC. In addition to having binding sites in the 3′-UTRs of their predicted targets, these 12 miRNAs were also inversely correlated with the expression levels of their predicted targets (FDR < 0.05, based on linear regression model, see Materials and Methods). As a result, we identified a master miRNA-gene regulatory network for PTC consisting of 12 miRNAs that can be visualized in Fig. 1. Such network reveals new candidate genes important for thyroid carcinogenesis. It also shows that some genes essential for thyroid differentiation are under the influence of this network (Fig. 1A, circles in red). The three miRNAs predicted to regulate the largest number of targets are miR-182, miR-146b-3p, and miR-34a (regulating 71, 66, and 65 targets, respectively; Fig. 1B).

Network analysis have shown that genes that are subject to extensive miRNAs regulation, referred as to target hubs, are more likely to be biologically relevant (30, 31). In addition, it has been shown that many TFs are among these target hubs and there is increasing evidence of reciprocal regulation between miRNAs and TFs as well as the existence of extensive coordination in the regulation of shared targets genes at the genome-scale level (32, 33). Considering only bioinformatics prediction, we found that 48 out of 217 (22%) of the target genes in PTC were predicted to be regulated by five or more miRNAs and were thus considered target hubs (Fig. 1A, circles with a thick edge in the center of the network and Fig. 1C). Similar results were obtained using a second algorithm, DIANAmicroT (Supplementary Fig. S3). Among these genes, several important tumor suppressors and TFs involved in human cancer were found (Supplementary Table S3). Of note, PAX8 is predicted to be modulated by five miRNAs revealing this nuclear protein as a target hub.

As miR-146b-5p and -3p are two of the most abundant upregulated miRNA in PTC, we focused our analysis on both strands generated by the same pre-miR. We found that miR-146b-5p and miR-146b-3p target 54 and 66 genes, respectively, being 22 of these genes targeted by both strands (Fig. 2A and B). The majority of these target genes are related to ECM–receptor interaction, CAMs and focal adhesion (Fig. 2C and Supplementary Table S4). Of note, miR-146b-3p targets two genes essential for thyroid differentiation, namely *PAX8* and *SLC5A5* (*NIS*; Fig. 2B, circles in red). In addition, miR-146b-5p targets *DIO2*, the iodothyronine deiodinase that converts T4 into T3; and both miR-146b-3p and -5p target *IYD* (*DEHAL1*), the iodotyrosine deiodinase that controls the recycling of iodide for thyroid hormone synthesis (Fig. 2B, circles in red). Overall, these results uncover the target genes of miR-146b-5p and -3p in PTC, revealing that this miRNA precursor is a key regulator of iodide-metabolizing genes. Interestingly, *SLC5A5* (*NIS*), *IYD* (*DEHAL1*), and *DIO2* are downstream targets of PAX8 (22, 34). Therefore, miR-146b regulates both the TF (PAX8) and its downstream target genes (*NIS*, *DEHAL1*, and *DIO2*), suggesting that miR-146b forms a feed-forward loop that controls gene expression through a direct and indirect mechanism (Fig. 2D).

Table 1. Most abundantly deregulated miRNAs in PTC

	Average normal (CPM)	Average tumoral (CPM)	Fold change	*P*	FDR
Upregulated miRNAs					
hsa-miR-146b-5p	1,811.75	79,891.84	35.9	2.05E−11	4.51E−09
hsa-miR-21-5p	14,129.65	56,835.03	3.8	9.15E−11	1.61E−08
hsa-miR-221-3p	1,179.28	11,301.82	9.4	4.51E−07	1.90E−05
hsa-miR-182-5p	2,972.44	8,713.77	3.0	4.91E−06	1.47E−04
hsa-miR-222-3p	753.77	6,641.46	8.6	1.03E−06	3.96E−05
hsa-let-7e-5p	1,773.24	2,839.12	1.8	3.37E−03	3.96E−02
hsa-miR-31-5p	309.46	1,911.69	7.5	4.51 E−08	2.84E−06
hsa-miR-21-3p[a]	415.64	1,600.11	3.6	7.43E−09	5.95E−07
hsa-miR-146b-3p	36.59	1,558.30	33.0	2.00E−12	5.88E−10
hsa-miR-375	237.74	1,390.84	21.4	3.15E−10	4.64E−08
hsa-miR-181a-2-3p[a]	462.86	809.28	1.9	4.95E−04	8.39E−03
hsa-miR-183-5p	213.81	724.28	3.1	1.68E−05	4.50E−04
hsa-miR-34a-5p	169.50	655.21	4.3	1.50E−12	5.88E−10
hsa-miR-155-5p	310.22	534.88	2.1	4.18E−03	4.72E−02
Downregulated miRNAs					
hsa-miR-451a	29,070.32	8,055.11	0.22	1.34E−08	9.83E−07
hsa-miR-486-5p	20,534.54	7,145.64	0.28	1.49E−06	5.25E−05
hsa-miR-100-5p	11,537.56	6,663.36	0.53	4.00E−03	4.58E−02
hsa-miR-30a-3p	2,548.37	1,394.93	0.56	2.50E−03	3.15E−02
hsa-miR-138-5p	2,223.51	718.55	0.31	9.06E−08	4.99E−06
hsa-miR-99a-5p	1,909.10	991.79	0.56	5.24E−04	8.41 E−03
hsa-miR-204-5p	1,180.71	191.41	0.15	2.40E−09	2.93E−07
hsa-miR-199b-5p	1,003.45	599.95	0.40	2.98E−03	3.66E−02

[a]miR-21-3p and miR-181a-2-3p are not included in TargetScan database.

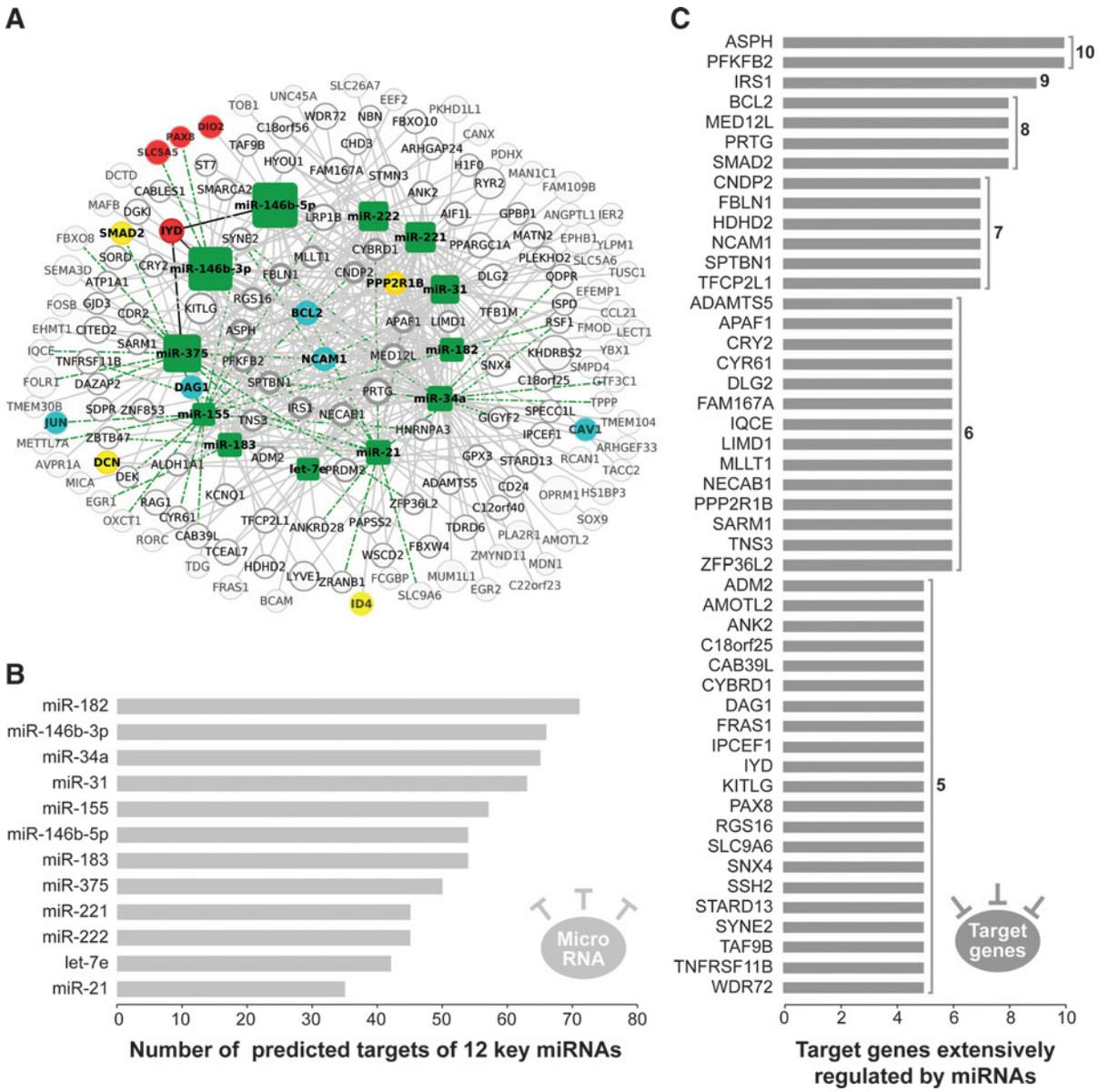

Figure 1.
Core miRNA-gene regulatory network including 12 key miRNAs and their targets in PTC. A, the miRNA-gene network drawn by Cytoscape 3 shows the relationships between 12 key miRNAs (green squares) and the genes they are predicted to regulate (circles). The size of the node is proportional to the fold change in the sequencing analysis. The thickness of the node edges is proportional to the number of predicted key miRNAs regulators; solid lines indicate significant inverse correlation; dotted lines indicate experimentally validated interactions; the colors in the circles indicate the annotated function of the gene (red, thyroid differentiation genes; blue, focal adhesion molecules; yellow, TGFβ signaling). As miR-21-3p and miR-181a-2-3p are not included in TargetScan database, they were not considered in this network. B, histogram showing the number of predicted targets for each of the 12 most abundant upregulated miRNAs. C, target genes with extensive regulation by miRNAs (≥5).

We wanted to extend our analysis to other miRNAs involved in thyroid differentiation. According to TargetScan, we found that a group of 11 upregulated miRNAs were predicted to target genes essential for thyroid differentiation (Supplementary Table S5). As mentioned before, PAX8 is predicted to be modulated by five miRNAs (miR-146b-3p, miR-182, miR-221, miR-222, and let-7e). However, downregulated miRNAs are also targeting *PAX8*, which might be counteracting the inhibitory effects mediated by the upregulated miRNAs. NIS is predicted to be modulated by miR-146b-3p and by miR-21-5p. FOXE1 is predicted to be modulated by miR-155 and TSHR by miR-34a, though other downregulated miRNAs are involved. TG seems not to be modulated by any deregulated miRNAs in PTC.

PAX8 and miR-146b cooperate in regulating shared targets genes and regulate each other

Both TFs and miRNAs can exert a widespread impact on gene expression. Network studies have revealed that miRNAs and TFs

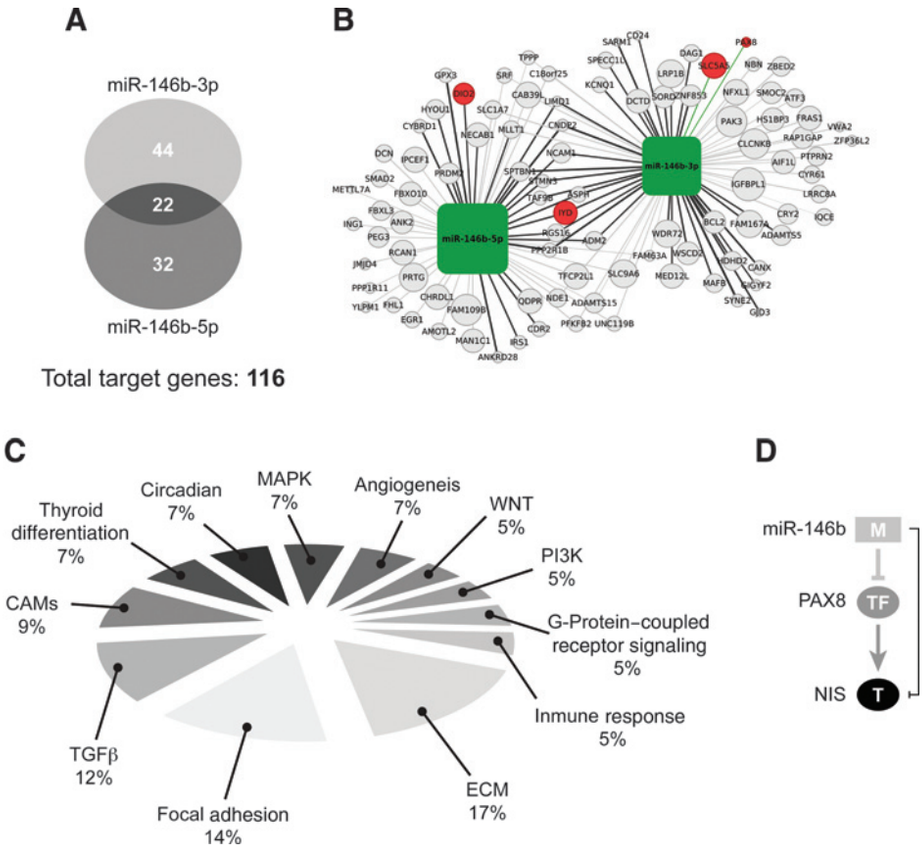

Figure 2.
Targetomes of miR-146b-5p and miR-146b-3p. A, Venn diagram of miR-146b-5p and -3p targets genes. B, miR-146b-gene expression network. The network drawn by Cytoscape 3 comprises 98 miRNA–gene interactions, involving 76 genes. The black, gray, and green lines indicate significant inverse correlation, only predicted and validated interactions, respectively. Line widths are proportional to the correlation coefficient. The size of the node is proportional to the fold change. The red circles correspond to iodide metabolizing genes (DIO2, IYD, and SLC5A5) and to the Pax8 TF. C, diagram showing percentage of the biologic processes related to the targetome of miR-146b-3p and miR-146b-5p. D, miR-146b-3p regulates the TF (PAX8) and its target (NIS), forming a feed-forward loop.

act coordinately to regulate sets of common target genes at the genome-scale level through the existence of reciprocal regulation between each other. More locally, such miRNAs–TF pairs may form small regulatory circuits that constitute successful mechanisms of gene expression in one particular organism or tissue. As mentioned before, we observed that miR-146b-3p was predicted to regulate both the TF (PAX8) and its downstream target gene (NIS). We therefore wanted to explore whether miR-146b and PAX8 shared more target genes in the sequencing data derived from the tumor samples. For this purpose, we used our previously characterization of the downstream targets genes of PAX8 in the rat thyroid cell line PCCl3 (22). We first confirmed that PAX8 was significantly downexpressed in the tumors (FC, 0.5; $P < 0.05$; not shown). We next searched in our sequence analysis and found that 51 downregulated genes in the tumors were downstream target genes of PAX8. Interestingly, PAX8 and miR-146b-3p shared 15 target genes including *SLC5A5* (*NIS*) and *IYD* (*DEHAL*; Fig. 3A and B).

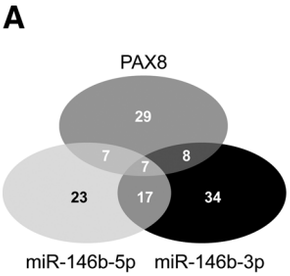

B

Shared target genes by PAX8 and 146b-5p	Shared target genes by PAX8 and 146b-3p	Shared target genes by PAX8 and both 146b
ANKRD28	*ASPH*	*CNDP2*
ASPH	*ATF3*	***IYD****
CNDP2	*CNDP2*	*PFKFB2*
DIO2*	*CYR61*	*PPP2R1B*
FHL1	*FAM167A*	*SPTBN1*
HYOU1	*HDHD2*	*ASPH*
IYD*	***IYD****	*NCAM1*
METTL7A	*NCAM1*	
NCAM1	*PFKFB2*	
QDPR	*PPP2R1B*	
PRDM2	*RAP1GAP*	
SPTBN1	*SORD*	
PFKFB2	*SPTBN1*	
PPP2R1B	*SYNE2*	
	SLC5A5*	

*Iodine metabolizing genes

Figure 3.
PAX8 and miR-146b cooperate in regulating shared targets. A, Venn diagram showing the number of common target genes of miR-146b-5p, miR-146b-3p, and PAX8 in PTC. B, list of target genes shared by PAX8 with each and with both strands of miR-146b. Those genes marked with stars indicate iodide metabolizing genes.

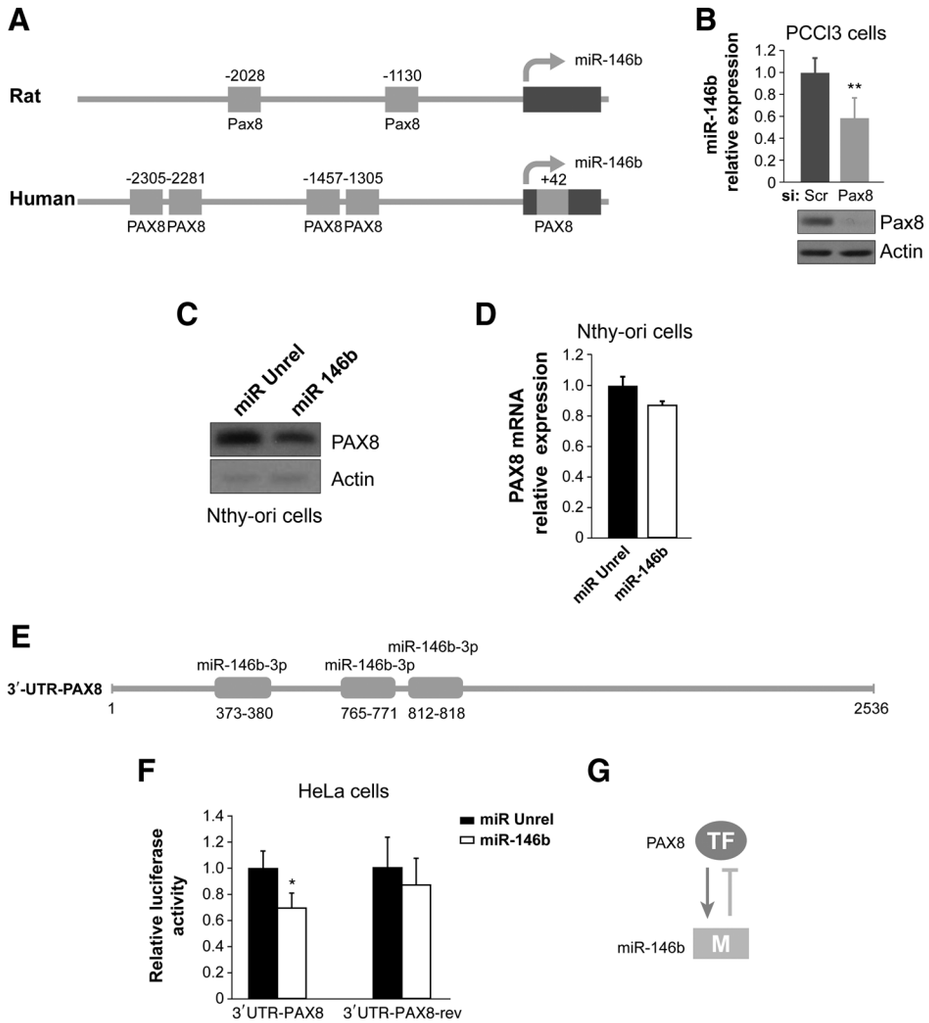

Figure 4.
miR-146b-3p and PAX8 regulate each other. A, schematic representation of miR-146b regulatory region showing the binding sites for PAX8 in rat and human genome. B, relative expression levels of miR-146b analyzed by qRT-PCR (top) in Pax8-silenced PCCl3 cells (siPax8) versus siScramble cells (Scr; bottom). The results are the means of three different experiments; bars represent SEM. C, a representative Western blot analysis for PAX8 protein extracted from Nthy-ori cells transfected with an unrelated pre-mir (pre-mir-373 or -15a) or with a pre-mir-146b expressing construct; actin protein was used as a loading control. D, qRT-PCR analysis of PAX8 mRNA levels performed in the same conditions as shown in C. E, schematic representation of PAX8 gene 3′-UTR with the three target sites for miR-146b-3p according to TargetScan. F, relative luciferase activity in HeLa cells transiently cotransfected with 3′-UTR–PAX8 or 3′-UTR–PAX8 reverse constructs along with pre-mir-146b or unrelated pre-mir (pre-mir-373 or -15a) expressing constructs, respectively. Relative activity of luciferase expression was normalized to a transfection control using *Renilla*. The results are the means of five different experiments; bars represent SEM. Statistical significance was evaluated by a two-tailed *t* test. Differences were considered significant at *, $P < 0.05$; **, $P < 0.01$ to 0.001; ***, $P < 0.001$. G, schematic representation of PAX8 and miR-146b regulating each other forming a feedback loop.

We next wanted to study whether PAX8 and miR-146b were regulating each other. To explore whether PAX8 regulates miR-146b expression, we first searched for putative binding sites of PAX8 in the miR-146b regulatory region. We found several PAX8-binding elements upstream the transcription start site of both rat and human miR-146b (Fig. 4A and Supplementary Dataset S4). We next studied the effect of Pax8 silencing on miR-146b expression after siRNA transfection in PCCl3 cells (Fig. 4B). We observed that the levels of miR-146b significantly decreased after silencing Pax8, suggesting that this TF positively regulates the transcription of miR-146b. The same results were obtained when Pax8 was silenced by shRNA (not shown).

Conversely, to explore whether miR-146b regulates PAX8 expression, Nthy-ori cells were transfected with an expression vector encoding for the miR-146b precursor, which expresses the two strands miR-146b-5p and miR-146-3p. Overexpression of miR-146b decreased the protein levels of endogenous PAX8 (Fig. 4C), yet no significant effect was observed in the mRNA levels (Fig. 4E). TargetScan-based bioinformatics predictions showed that there were three putative binding sites in the 3′-UTR of *PAX8* for miR-146b-3p (Fig. 4E). Moreover, we addressed whether miR-146b-3p was specifically targeting the 3′-UTR of *PAX8*. We thus generated a luciferase reporter vector encoding for the entire 3′-UTR and another one for the 3′-UTR reverse, used as a negative control. Using HeLa cells, we observed that miR-146b overexpression induced a 30% decrease of the luciferase activity on average of the entire 3′-UTR of *PAX8* (Fig. 4F). These results show that miR-146b-3p directly represses *PAX8* expression by targeting the 3′-UTR. And overall, we provide evidence whereby in thyroid cells operate a negative feedback loop in which the TF (PAX8) limits its own activity by inducing a repressor (miR-146b; Fig. 4G).

miR-146b-3p decreases NIS expression by targeting the 3′-UTR and is regulated by TSH

To explore whether miR-146b-3p was able to downregulate NIS expression, we first used MDCKhNIS. This cell system expresses NIS in the cell membrane and mediates active transport of iodide into the cytoplasm (24). We transfected these cells an expression vector encoding for the miR-146b precursor. We observed that miR-146b decreases protein levels of NIS (Fig. 5A), yet no significant effect was observed in the mRNA levels (Fig. 5B). In addition, an 80% reduction in iodide uptake was seen (Fig. 5C). These

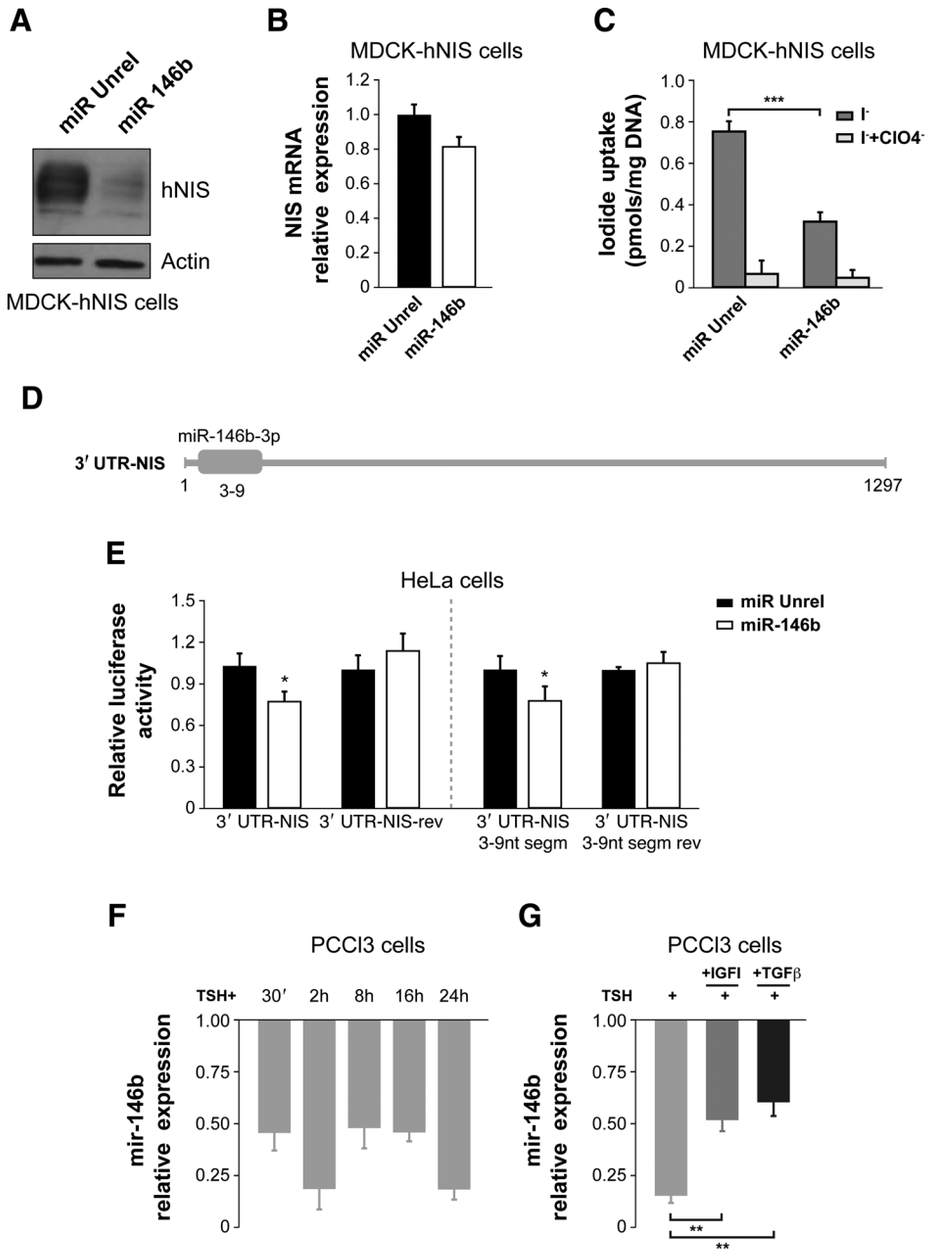

Figure 5.
miR-146b-3p targets NIS and is downregulated by TSH. A, representative Western blot analyses for NIS and actin protein as a loading control. Proteins were extracted from MDCK-hNIS transfected with an unrelated pre-mir (pre-mir-373 or -15a) or with a pre-mir-146b–expressing constructs. B, qRT-PCR analysis of NIS mRNA levels in the same conditions shown in A. C, NIS activity determined by iodide uptake after transfecting MDCK-hNIS cells with pre-mir-146b or the unrelated expressing construct. Perchlorate ($ClO4^-$) was used as a competitive inhibitor of iodide uptake mediated by NIS. Each bar represents the mean ± SE from three independent experiments performed in triplicate. D, schematic representation of NIS gene 3′-UTR target site for miR-146b-3p. E, relative luciferase activity in HeLa cells transiently cotransfected with 3′-UTR-hNIS or 3′-UTR-hNIS 3–9 nt segment constructs along with pre-mir-146b or unrelated pre-mir expressing construct, respectively. Relative activity of luciferase expression was normalized to a transfection control using *Renilla*. The results are the means of five different experiments; bars represent SEM. F, qRT-PCR analysis of miR-146b was carried out on PCCl3 cells treated with TSH (0.5 mU/mL) at the indicated times. The relative expression values indicate the relative change in the expression levels between PCCl3 cells treated with TSH and PCCl3 maintained in starvation medium (not treated with TSH). G, qRT-PCR analysis of miR-146b in PCCl 3 cells treated for 2 hours with TSH or TSH plus IGF1 or TFGβ at the doses (100 or 10 ng/mL, respectively). Each bar represents the mean ± SE from three independent experiments performed in triplicate. Statistical significance was evaluated by a two-tailed *t* test. Differences were considered significant at *, $P < 0.05$; **, $P < 0.01$ to 0.001; ***, $P < 0.001$.

results show that miR-146b impairs NIS mRNA translation and subsequently decreases protein levels and transport activity of NIS.

We next wanted to address whether miR-146b-3p was specifically targeting the 3′-UTR of h*NIS*. The bioinformatics predictions informed us that one putative target site was present at positions 3-9 in the 3′-UTR (Fig. 5E). We generated a luciferase reporter vector encoding for the entire 3′-UTR and another one encoding for a short region of 7nt in tandem harboring the target site at positions 3–9 (called 3–9 nt segm). The reverse constructs of the entire 3′-UTR and the 3–9 nt segm were used as negative controls. After transfecting HeLa cells, we observed a 25% decrease of the luciferase activity on average both with the entire 3′-UTR and the 3–9 nt segm when we transfected cells with miR-146b (Fig. 5E). These results provide evidence that the direct repression of NIS expression by miR-146b-3p requires a binding site at positions 3–9 of the 3′-UTR.

We finally wanted to investigate whether miR-146b was hormonally regulated in differentiated thyroid cells. TSH is essential for the thyroid cell to express the genes involved in the uptake and metabolism of iodide and hence, allows the thyroid cell to be fully differentiated. Thus, we assumed that those miRNAs more likely to be involved in targeting thyroid differentiating genes are necessarily downregulated by TSH in normal thyroid cells. To explore whether the expression of miR-146b was dependent on TSH regulation, we used rat PCCl3 cells. miR-146b was strongly

downregulated after stimulating the cells with TSH (Fig. 5F). In addition, this downregulation was recovered by IGFI and TGFβ, known repressors of TSH-induced NIS expression (Fig. 5G; refs. 35, 36). Thus, endogenous levels of miR-146b are tightly controlled by TSH in differentiated thyroid cells.

Discussion

In this work, we identified a master miRNA regulatory network in PTC that is involved in essential biologic processes such as differentiation. Functional studies characterized miR-146b-3p as a repressor of PAX8 and NIS and showed that miR-146b and PAX8 regulate each other, unveiling a regulatory circuit that determines the differentiated phenotype in PTC.

Identifying the molecular events leading to the loss of thyroid differentiation in thyroid cancer attracts much attention, particularly loss of NIS expression. NIS mediates active transport of iodide into the thyroid cell, the basis for the diagnosis and therapeutic management of thyroid cancer patients with radioiodide. We demonstrate for the first time that NIS is posttranscriptionally modulated by miRNAs in thyroid cancer. Very recently, it has been shown that miR-339 modulates NIS expression in rat normal thyroid cells (37), yet this miRNA has not been shown to be deregulated in thyroid cancer in previous studies including ours (16, 38, 39). We consistently show that miR-146b-3p binds to the 3′-UTR of *NIS* (site 3–9 nt), leading to an impaired translation of the protein and subsequently decreasing the iodide uptake of the cells. Several mechanisms have been proposed to explain NIS repression in thyroid cancer in order to establish new therapeutic approaches to try to reinduce iodide uptake (8, 40). All of them are based on the transcriptional repression induced by aberrant signaling pathways and/or epigenetic events. Here, we show an additional mechanism based on the posttranscriptional regulation of NIS mediated by miRNAs.

We also show that miR-146b-3p is strongly downregulated by TSH in normal thyroid cells (PCCl3) and its expression is recovered by IGF1 and TGFβ, two known repressors of NIS expression via PI3K and Smads, respectively (35, 36). This highlights the importance of a tight hormonal regulation of miRNA expression in the thyroid cell. In accordance, it has been previously demonstrated that TSH signaling through CREB1 represses several miRNAs by physically interacting with their regulatory region (41). As TSH signaling is impaired during thyroid carcinogenesis, the miRNAs are able to escape from this TSH-mediated repression. In addition to the impairment of TSH signaling, TGFβ and PI3K signaling are known to be hyperactivated in thyroid cancer (8, 42). Thus, we suggest that aberrant signaling of key growth factors and cytokines (i.e., TSH, TGFβ, and IGF1) are contributing to the strong upregulation of miR-146b seen in thyroid cancer (up to 35-fold).

Apart from regulating NIS, the most abundant miRNAs are involved in the modulation of other genes essential for thyroid differentiation. PAX8 is a TF that specifically governs the transcription of NIS and is necessary for the development of the thyroid gland and for maintaining the differentiated state in the thyroid of the adult. Moreover, this TF is a master regulator of other key cellular processes such as cell-cycle regulation, DNA repair, replication, metabolism, and cell polarity (22, 43). We

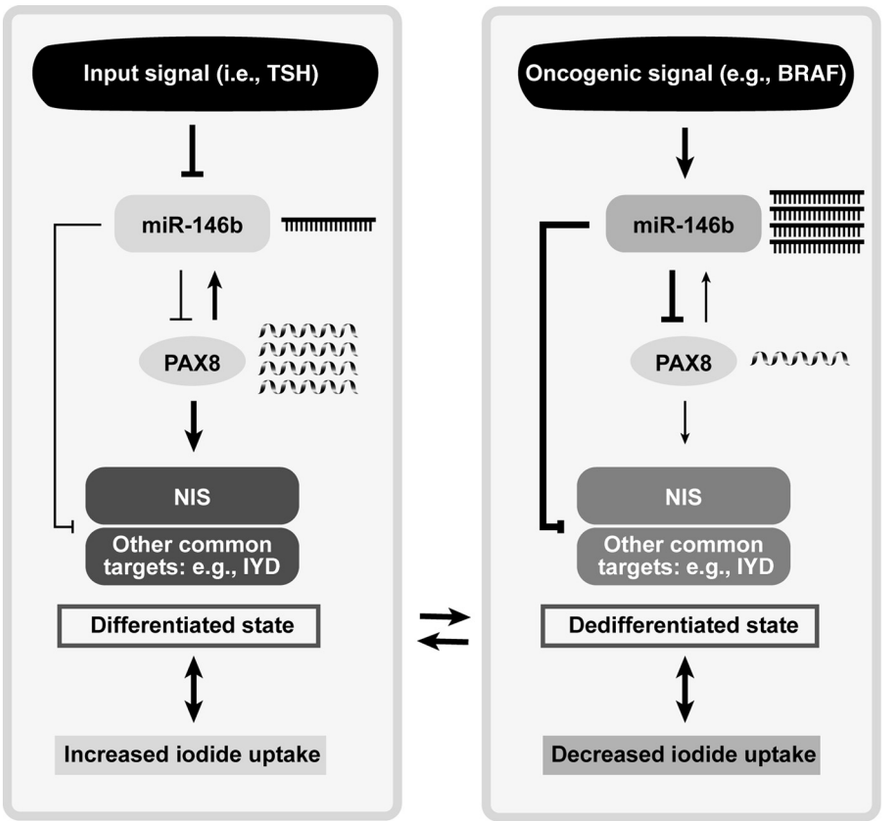

Figure 6.
Integrated model operating to determine the thyroid differentiated state and subsequent iodide uptake. The differentiated state of thyroid cells depends on an adequate TSH signaling. In such conditions, the cells show lower levels of miR-146b and higher levels of PAX8. Upon an oncogenic signal, TSH signaling is impaired and miR-146b expression is markedly increased, leading to a repression of PAX8 and their common targets such as NIS. As a result, tumor cells adopt a less differentiated state that, for instance, makes them more insensitive to radioactive iodide.

show that PAX8 is predicted to be targeted by five of the most abundant upregulated miRNAs in thyroid cancer (Fig. 1C and Supplementary Table S3), suggesting that this TF is a target hub that is in accordance with its biologic importance in the thyroid gland. One of such miRNAs, miR-146b-3p, effectively represses PAX8 through binding to its 3′-UTR. Intriguingly, we further show that PAX8 and miR-146b regulate each other and share common targets, including iodide metabolizing genes. This provides evidence that such miR-TF pair forms small regulatory circuits that constitutes a successful mechanism of regulating gene expression in the thyroid.

Regulatory circuits involving miRNAs and TFs are prevalent mechanisms of gene expression at the genome scale-level (44, 45). One of such regulatory circuits is the feed-forward loop where the miRNA simultaneously represses the TF and its target genes. This circuit functions to suppress leaky transcription and hence target genes will only be expressed whether the levels of the miRNA decrease. Here, we describe a miR-146b–PAX8–NIS circuit as an example of a feed-forward loop (Figs. 2E and 6) in which the miRNA (146b) represses the TF (PAX8) and its downstream target (NIS; Fig. 2E). In addition and complementary to this feed-forward loop, we also describe another regulatory circuit in which miR-146b and PAX8 form a negative feedback loop where the TF (PAX8) limits its own activity by inducing a repressor (miR-146b; Fig. 4G). Such a loop can result in coexpression of both components, either in steady-state levels or in oscillation. (46). The expression of both components depends on additional input signals. As a consequence, network circuits allow the spreading of regulatory effects. An upstream signal activates the miRNA, which, in turn, represses all its direct targets including the TF. As a result, all downstream targets of the TF are also repressed. In thyroid cells, the spreading of regulatory effects concerning PAX8 and miR-146b affect key biologic functions such as thyroid differentiation. Particularly, common target genes, such as *SLC5A5* (NIS), *IYD (*DEHAL), and *DIO2*, reveal the importance of controlling the expression of a set of genes regulating the metabolism of iodide.

Taken together, we propose an integrated model that may be operating to determine the thyroid differentiated phenotype and in the end, the uptake of iodide (Fig. 6). Thyroid cells are under the control of TSH and show lower levels of miR-146b and higher levels of PAX8. Upon an oncogenic signal (e.g., *BRAF*), TSH signaling is impaired and TGFβ and PI3K signaling hyperactivated, leading to higher levels of miR-146b and lower levels of PAX8. As a result, tumor cells adopt a less differentiated state that, for instance, makes them more insensitive to radioactive iodide. However, this state can change if an external signal transiently overcomes the oncogenic signal by decreasing the levels of the miR-146b. An example of such an external signal can be exogenous administration of recombinant human TSH, which is widely used in the clinical practice to enhance iodide uptake in thyroid cancer patients. Another example of an external signal that may promote a change in the differentiated state is kinase inhibitors (i.e., selumetinib).

We also unveiled for the first time the main target genes of miR-146b-5p and 146b-3p in PTC, both of them strands generated by the miR-146b precursor. As previously shown by other studies (39, 47), both strands are significantly upregulated in PTC, indicating that the 3p strand, although suffering degradation, reaches the minimum threshold amount to be considered as functional. miR-146b has been demonstrated to be a prognostic factor for PTC as it is associated with aggressive clinicopathologic features and a poor clinical outcome (48). It has also been proven to be elevated in the serum of patients with PTC (49). Some of its target genes have been validated in thyroid cancer (50). Thus, although more functional studies are needed, particularly in animal models, we believe that miR-146b can be currently considered as an oncomir in thyroid cancer. Our results contribute to this notion as we demonstrate that one of the strands specifically targets NIS and PAX8, key players in the dedifferentiation process occurring in thyroid cancer.

In contrast to expression profiling based on microarrays, next-generation sequencing enables the study of miRNAs at unprecedented quantitative and qualitative accuracy. As mentioned before, quantitative analysis helps to discriminate those miRNAs more functionally prominent. In fact, over 60% of detected miRNAs have no real activity, indicating that the functional miRNome of a cell is considerably smaller than previously thought (15). In addition, it allows the characterization of both the 3p and 5p mature strands of a given miRNA. The first study performing next-generation sequencing of miRNAs in PTC mainly focused on isomer analysis (39). In another recent study, Huang and colleagues (38) analyzed the miRNAs expression datasets of PTC from TCGA Data Portal. The authors emphasized that immune responses are significantly enriched and under specific regulation in the direct miRNA–target network, but miRNAs regulating thyroid differentiation genes were not addressed. Very recently, while preparing this article, a study based on TCGA (16) showed that three selected miRNAs that were epigenetically regulated (miR-21, miR-146b, and miR-204) contributed to loss of thyroid differentiation as they correlated to gene expression data for nine thyroid genes including NIS (but not PAX8). However, functional studies proving the impact of miRNAs in thyroid differentiation are needed. In our work, we went one step further and provide functional evidence for the requirement of miR-146b-3p as a key player in loss of thyroid differentiation in PTC.

In summary, we present in this work the functional miRNomes of normal thyroid and PTC tumors, providing resources for investigating the regulatory roles of miRNAs in thyroid biology and thyroid carcinogenesis. Such miRNAs play important functions as they generate regulatory circuits that modulate genes essential for thyroid differentiation. We provide evidence to consider the regulatory circuit based on miR-146b-3p–PAX8–NIS as a regulator of the differentiated state in thyroid tumor cells. Therefore, inhibition of the miR-146b, one of the key miRNAs in the network, may represent an important strategy for the treatment of PTC, particularly to reinduce the uptake of radioactive iodide in patients.

Disclosure of Potential Conflicts of Interest

No potential conflicts of interest were disclosed.

Authors' Contributions

Conception and design: G. Riesco-Eizaguirre, L. Wert-Lamas, P. Santisteban

Development of methodology: G. Riesco-Eizaguirre, L. Wert-Lamas, L.P. Fernández

Acquisition of data (provided animals, acquired and managed patients, provided facilities, etc.): G. Riesco-Eizaguirre, L. Wert-Lamas, A. Sastre-Perona, P. Santisteban

Analysis and interpretation of data (e.g., statistical analysis, biostatistics, computational analysis): G. Riesco-Eizaguirre, L. Wert-Lamas, J. Perales-Patón, P. Santisteban

Writing, review, and/or revision of the manuscript: G. Riesco-Eizaguirre, L. Wert-Lamas, A. Sastre-Perona, P. Santisteban

Administrative, technical, or material support (i.e., reporting or organizing data, constructing databases): G. Riesco-Eizaguirre, J. Perales-Patón, P. Santisteban
Study supervision: G. Riesco-Eizaguirre, P. Santisteban

Acknowledgments

The authors thank Antonio De la Vieja for critical reading of the article. They also thank Dr. Nancy Carrasco (Department of Cellular and Molecular Physiology, Yale School of Medicine) for providing the human and rat NIS antibody.

Grant Support

This work was supported by Grants BFU2010-16025 and SAF2013-44709-R from the Dirección General de Proyectos de Investigación; RD12/0036/0030 from FIS, Instituto de Salud Carlos III (ISCIII); and S2011/BMD-2328 TIRONET project from the Comunidad de Madrid (Spain) to P. Santisteban; and FIS-ISCIII; PI14/01980 to G. Riesco-Eizaguirre. L. Wert-Lamas and A. Sastre-Perona hold a predoctoral FPI and FPU fellowship, respectively, from the Spanish Government and L.P. Fernández was a JAE.doc postdoctoral from CSIC.

The costs of publication of this article were defrayed in part by the payment of page charges. This article must therefore be hereby marked *advertisement* in accordance with 18 U.S.C. Section 1734 solely to indicate this fact.

Received December 9, 2014; revised June 15, 2015; accepted July 13, 2015; published OnlineFirst August 17, 2015.

References

1. American Thyroid Association (ATA) Guidelines Taskforce on Thyroid Nodules and Differentiated Thyroid Cancer. Cooper DS, Doherty GM, Haugen BR, Kloos RT, Lee SL, et al. Revised American Thyroid Association management guidelines for patients with thyroid nodules and differentiated thyroid cancer. Thyroid 2009;19:1167–214.
2. Durante C, Haddy N, Baudin E, Leboulleux S, Hartl D, Travagli JP, et al. Long-term outcome of 444 patients with distant metastases from papillary and follicular thyroid carcinoma: benefits and limits of radioiodine therapy. J Clin Endocrinol Metab 2006;91:2892–9.
3. Pasca di Magliano M, Di Lauro R, Zannini M. Pax8 has a key role in thyroid cell differentiation. Proc Natl Acad Sci U S A 2000;97:13144–9.
4. Fernandez LP, Lopez-Marquez A, Santisteban P. Thyroid transcription factors in development, differentiation and disease. Nat Rev Endocrinol 2015;11:29–42.
5. Ohno M, Zannini M, Levy O, Carrasco N, di Lauro R. The paired-domain transcription factor Pax8 binds to the upstream enhancer of the rat sodium/iodide symporter gene and participates in both thyroid-specific and cyclic-AMP-dependent transcription. Mol Cell Biol 1999;19:2051–60.
6. Dai G, Levy O, Carrasco N. Cloning and characterization of the thyroid iodide transporter. Nature 1996;379:458–60.
7. Riesco-Eizaguirre G, Santisteban P. A perspective view of sodium iodide symporter research and its clinical implications. Eur J Endocrinol 2006;155:495–512.
8. Spitzweg C, Bible KC, Hofbauer LC, Morris JC. Advanced radioiodine-refractory differentiated thyroid cancer: the sodium iodide symporter and other emerging therapeutic targets. Lancet Diabetes Endocrinol 2014;2:830–42.
9. Kozomara A, Griffiths-Jones S. miRBase: annotating high confidence microRNAs using deep sequencing data. Nucleic Acids Res 2014;42:D68–73.
10. He H, Jazdzewski K, Li W, Liyanarachchi S, Nagy R, Volinia S, et al. The role of microRNA genes in papillary thyroid carcinoma. Proc Natl Acad Sci U S A 2005;102:19075–80.
11. Pallante P, Battista S, Pierantoni GM, Fusco A. Deregulation of microRNA expression in thyroid neoplasias. Nat Rev Endocrinol 2014;10:88–101.
12. Brown BD, Gentner B, Cantore A, Colleoni S, Amendola M, Zingale A, et al. Endogenous microRNA can be broadly exploited to regulate transgene expression according to tissue, lineage and differentiation state. Nat Biotechnol 2007;25:1457–67.
13. Sarasin-Filipowicz M, Krol J, Markiewicz I, Heim MH, Filipowicz W. Decreased levels of microRNA miR-122 in individuals with hepatitis C responding poorly to interferon therapy. Nat Med 2009;15:31–3.
14. Hou J, Lin L, Zhou W, Wang Z, Ding G, Dong Q, et al. Identification of miRNomes in human liver and hepatocellular carcinoma reveals miR-199a/b-3p as therapeutic target for hepatocellular carcinoma. Cancer Cell 2011;19:232–43.
15. Mullokandov G, Baccarini A, Ruzo A, Jayaprakash AD, Tung N, Israelow B, et al. High-throughput assessment of microRNA activity and function using microRNA sensor and decoy libraries. Nat Methods 2012;9:840–6.
16. Cancer Genome Atlas Research Network. Integrated genomic characterization of papillary thyroid carcinoma. Cell 2014;159:676–90.
17. Langmead B, Trapnell C, Pop M, Salzberg SL. Ultrafast and memory-efficient alignment of short DNA sequences to the human genome. Genome Biol 2009;10:R25.
18. Trapnell C, Pachter L, Salzberg SL. TopHat: discovering splice junctions with RNA-Seq. Bioinformatics 2009;25:1105–11.
19. Anders S, Pyl PT, Huber W. HTSeq-a Python framework to work with high-throughput sequencing data. Bioinformatics 2015;31:166–9.
20. Grimson A, Farh KK, Johnston WK, Garrett-Engele P, Lim LP, Bartel DP. MicroRNA targeting specificity in mammals: determinants beyond seed pairing. Mol Cell 2007;27:91–105.
21. Shannon P, Markiel A, Ozier O, Baliga NS, Wang JT, Ramage D, et al. Cytoscape: a software environment for integrated models of biomolecular interaction networks. Genome Res 2003;13:2498–504.
22. Ruiz-Llorente S, Carrillo Santa de Pau E, Sastre-Perona A, Montero-Conde C, Gomez-Lopez G, Fagin JA, et al. Genome-wide analysis of Pax8 binding provides new insights into thyroid functions. BMC Genomics 2012;13:147.
23. Sastre-Perona A, Santisteban P. Wnt-independent role of beta-catenin in thyroid cell proliferation and differentiation. Mol Endocrinol 2014;28:681–95.
24. Zuckier LS, Dohan O, Li Y, Chang CJ, Carrasco N, Dadachova E. Kinetics of perrhenate uptake and comparative biodistribution of perrhenate, pertechnetate, and iodide by NaI symporter-expressing tissues *in vivo*. J Nucl Med 2004;45:500–7.
25. De la Vieja A, Ginter CS, Carrasco N. Molecular analysis of a congenital iodide transport defect: G543E impairs maturation and trafficking of the Na^+/I^- symporter. Mol Endocrinol 2005;19:2847–58.
26. Robinson MD, McCarthy DJ, Smyth GK. edgeR: a Bioconductor package for differential expression analysis of digital gene expression data. Bioinformatics 2010;26:139–40.
27. Robinson MD, Oshlack A. A scaling normalization method for differential expression analysis of RNA-seq data. Genome Biol 2010;11:R25.
28. Young MD, Wakefield MJ, Smyth GK, Oshlack A. Gene ontology analysis for RNA-seq: accounting for selection bias. Genome Biol 2010;11:R14.
29. Chudova D, Wilde JI, Wang ET, Wang H, Rabbee N, Egidio CM, et al. Molecular classification of thyroid nodules using high-dimensionality genomic data. J Clin Endocrinol Metab 2010;95:5296–304.
30. Liang H, Li WH. MicroRNA regulation of human protein protein interaction network. RNA 2007;13:1402–8.
31. Budd WT, Weaver DE, Anderson J, Zehner ZE. microRNA dysregulation in prostate cancer: network analysis reveals preferential regulation of highly connected nodes. Chem Biodivers 2012;9:857–67.
32. Martinez NJ, Ow MC, Barrasa MI, Hammell M, Sequerra R, Doucette-Stamm L, et al. A *C. elegans* genome-scale microRNA network contains composite feedback motifs with high flux capacity. Genes Dev 2008;22:2535–49.
33. Tsang J, Zhu J, van Oudenaarden A. MicroRNA-mediated feedback and feedforward loops are recurrent network motifs in mammals. Mol Cell 2007;26:753–67.
34. Di Palma T, Conti A, de Cristofaro T, Scala S, Nitsch L, Zannini M. Identification of novel Pax8 targets in FRTL-5 thyroid cells by gene silencing and expression microarray analysis. PLoS ONE 2011;6:e25162.

35. Garcia B, Santisteban P. PI3K is involved in the IGF-I inhibition of TSH-induced sodium/iodide symporter gene expression. Mol Endocrinol 2002;16:342–52.
36. Costamagna E, Garcia B, Santisteban P. The functional interaction between the paired domain transcription factor Pax8 and Smad3 is involved in transforming growth factor-beta repression of the sodium/iodide symporter gene. J Biol Chem 2004;279:3439–46.
37. Lakshmanan A, Wojcicka A, Kotlarek M, Zhang X, Jazdzewski K, Jhiang S. microRNA-339-5p modulates Na^+/I^- symporter-mediated radioiodide uptake. Endocr Relat Cancer 2015;22:11–21.
38. Huang CT, Oyang YJ, Huang HC, Juan HF. MicroRNA-mediated networks underlie immune response regulation in papillary thyroid carcinoma. Sci Rep 2014;4:6495.
39. Swierniak M, Wojcicka A, Czetwertynska M, Stachlewska E, Maciag M, Wiechno W, et al. In-depth characterization of the microRNA transcriptome in normal thyroid and papillary thyroid carcinoma. J Clin Endocrinol Metab 2013;98:E1401–9.
40. Portulano C, Paroder-Belenitsky M, Carrasco N. The Na^+/I^- symporter (NIS): mechanism and medical impact. Endocr Rev 2014;35:106–49.
41. Leone V, D'Angelo D, Ferraro A, Pallante P, Rubio I, Santoro M, et al. A TSH-CREB1-microRNA loop is required for thyroid cell growth. Mol Endocrinol 2011;25:1819–30.
42. Riesco-Eizaguirre G, Rodriguez I, De la Vieja A, Costamagna E, Carrasco N, Nistal M, et al. The BRAFV600E oncogene induces transforming growth factor beta secretion leading to sodium iodide symporter repression and increased malignancy in thyroid cancer. Cancer Res 2009;69:8317–25.
43. Di Palma T, Filippone MG, Pierantoni GM, Fusco A, Soddu S, Zannini M. Pax8 has a critical role in epithelial cell survival and proliferation. Cell Death Dis 2013;4:e729.
44. Herranz H, Cohen SM. MicroRNAs and gene regulatory networks: managing the impact of noise in biological systems. Genes Dev 2010;24:1339–44.
45. Shalgi R, Lieber D, Oren M, Pilpel Y. Global and local architecture of the mammalian microRNA-transcription factor regulatory network. PLoS Comput Biol 2007;3:e131.
46. Martinez NJ, Walhout AJ. The interplay between transcription factors and microRNAs in genome-scale regulatory networks. Bioessays 2009;31:435–45.
47. Dettmer M, Perren A, Moch H, Komminoth P, Nikiforov YE, Nikiforova MN. Comprehensive MicroRNA expression profiling identifies novel markers in follicular variant of papillary thyroid carcinoma. Thyroid 2013;23:1383–9.
48. Chou CK, Yang KD, Chou FF, Huang CC, Lan YW, Lee YF, et al. Prognostic implications of miR-146b expression and its functional role in papillary thyroid carcinoma. J Clin Endocrinol Metab 2013;98:E196–205.
49. Lee JC, Zhao JT, Clifton-Bligh RJ, Gill A, Gundara JS, Ip JC, et al. MicroRNA-222 and microRNA-146b are tissue and circulating biomarkers of recurrent papillary thyroid cancer. Cancer 2013;119:4358–65.
50. Geraldo MV, Yamashita AS, Kimura ET. MicroRNA miR-146b-5p regulates signal transduction of TGF-beta by repressing SMAD4 in thyroid cancer. Oncogene 2012;31:1910–22.